RSC Advances

PAPER

View Article Online
View Journal | View Issue

Cite this: *RSC Adv.*, 2022, **12**, 4703

Insights into the effect of distal histidine and water hydrogen bonding on NO ligation to ferrous and ferric heme: a DFT study†

Fatemeh Fateminasab,[a] Aurelien de la Lande [b] and Reza Omidyan *[a]

The effect of distal histidine on ligation of NO to ferrous and ferric-heme, has been investigated with the high-level density functional theoretical (DFT) method. It has been predicted that the distal histidine significantly stabilizes the interaction of NO ferrous-heme (by −2.70 kcal mol^{-1}). Also, water hydrogen bonding is quite effective in strengthening the Fe–NO bond in ferrous heme. In contrast in ferric heme, due to the large distance between the H_2O and O(NO) and lack of hydrogen bonding, the distal histidine exhibits only a slight effect on the binding of NO to the ferric analogue. Concerning the bond nature of Fe^{II}–NO and Fe^{III}–NO in heme, a QTAIM analysis predicts a partially covalent and ionic bond nature in both systems.

Received 16th November 2021
Accepted 30th January 2022

DOI: 10.1039/d1ra08398h

rsc.li/rsc-advances

1. Introduction

Hemoproteins are a vital component of the human body where they play a crucial role.[1] Hemes, the iron complexes of porphyrins have an extensive variety of structures and functions, including electron and proton transfer,[2] oxidation of substrates,[3] transport and storage of metal ions,[4] and aerobic breathing.[5] Moreover, ligation of dual and more atomic ligands such as O_2, N_2, NO, CO and H_2O affects the function of hemoproteins such as detection, tracking, transport and storage.[1,6] Myoglobin (MB) and hemoglobin (HB) transport molecular oxygen in vertebrate blood and muscle cells respectively. The active site of these hemeproteins is the heme B, prosthetic group. Naturally in biological systems, especially MB and HB, iron is found in the common oxidation states including ferrous (Fe^{II}) and ferric (Fe^{III}). HB and MB can coordinate CO, NO, O_2 in the reduced state, Fe^{II}, and also in an oxidized state, Fe^{III}, binds H_2O and small anionic ligands (*e.g.* CN^-, SCN^-, F^-).[6] In MB, four N atoms at the equatorial position, one or two ligand groups at the axial sites, could be coordinated the iron cation.[7] In the proximal site of MB, the fifth coordination site is accomplished by the imidazole ring of a histidine residue (HIS93) and thus the heme group binds to this protein. Moreover, a distal histidine residue (HIS64) is located near the opposite side in the right position. The distal HIS group is not directly bound to iron but can stabilize the sixth ligand by hydrogen bonding. This hydrogen bond plays a key role in the selectivity of the heme group to adsorb different ligands.[6,8]

The diatomic NO$^\bullet$ radical, being toxic and corrosive, is an important molecule that is produced, sensed, and detoxified by heme proteins. It plays a vital role in mammals both as a means of immune defense *versus* pathogens and as a signaling molecule in the cardiovascular organ system and the brain.[9] The effect of native distal group (HIS64) and other residues as a distal group into NO, has been studied experimentally and computationally by different groups.[10–15] It has been shown that the Fe^{II}–N–O angle is bent (~140°), while Fe^{III}–N–O is linear (~180°).[16] Olson *et al.*[10] reported that ligation of NO to heme is stabilized several times using hydrogen bonding to HIS64. Moreover, by replacing of distal group from HIS64 to apolar residues and the association and dissociation rate constants of NO to iron exhibit slight alterations.[10]

From a computational perspective, Blomberg and co-workers[13] investigated the geometric structures for the binding of O_2, NO, and CO to ferrous-heme in three models by Density Functional Theory (DFT) calculations with the B3LYP exchange-correlation (XC) functional. They calculated the Gibbs free energy of binding of O_2, NO, and CO for three models (*i.e.* free porphyrin, myoglobin and cytochrome oxidase). Spiro proposed that the distal HIS64 is allowed to rotate out of its plane, thus it moves closer to the N atom of ligated NO and both the O, and N atoms of NO could be involved in hydrogen bonds with H of HIS64.[16] Praneeth *et al.*[17] investigated the interaction between 5-coordinated ferric-hemes with bound NO and axial imidazole ligands both theoretically and experimentally. By DFT calculations, the low spin (LS) Fe^{III}–NO(radical) ($S = 0$), LS Fe^{II}–NO^+ ($S = 1/2$) and high spin (HS) Fe^{III}–NO(radical) ($S = 2$) states were compared. These results indicated that the properties of these low spin states have differed from each other and also the HS

[a]*Department of Chemistry, University of Isfahan, 81746-73441 Isfahan, Iran. E-mail: r.omidyan@sci.ui.ac.ir; rezaomidyan51@gmail.com; Fax: +98 31 3668 9732*

[b]*Université Paris-Saclay, CNRS, Institut de Chimie Physique, UMR8000, 91405, Orsay, France*

† Electronic supplementary information (ESI) available. See DOI: 10.1039/d1ra08398h

Fe^{III}–NO(radical) state has a weak Fe–NO bond.[18] These results were confirmed by Hunt and Lehnert.[18] The binding energies of FeP(Im)-AB (AB = NO, O_2 and CO, imidazole) evaluated with different density functional models by Liao *et al.*[19] The results showed different values for bonding energy in these systems.[19] In the other work, Liao and coworkers[15] investigated the binding of NO, and O_2 to heme in heme-nitric oxide proteins with DFT and dispersion-corrected DFT methods. Also, the local protein environment has been determined by considering the six nearest surrounding residues in the investigated systems. Particularly, the effects of the distal HIS64 (MB) have been also investigated on the proximal Fe–HIS binding. The heme-AB (AB = O_2, NO) binding energies in iron porphyrin FeP(His)(AB) and myoglobin Mb(AB) were determined. However, and to the best of our knowledge, the effects of neighboring amino acids (*e.g.* histidine) and solvent on the energy and nature of NO interaction to heme are not fully understood yet. In this study, a comprehensive density functional theory (DFT) and QTAIM analysis, have been employed to investigate the mentioned issues as well. As stated in previous reports on the interaction of NO to Fe-porphyrin and Mb (in absence and presence of distal His), the protein environment in Mb has slight effect on the heme-NO binding strength.[15,20,21]

In this study, we have considered a simplified porphyrin-iron model to decrease the computation costs. This model has been examined in our previous work (comparing to experiment) and it has been established the model is capable enough to describe the binding of small ligands to heme.[22] Also, it retains the central feature of heme and has been used widely in previous computational and theoretical studies,[24,37,38] and it has been emphasized that this model is accurate enough for investigation of ligand to heme interactions. The notations of $[Fe^{II}P]$, $[Fe^{III}P]^+$, $[Fe^{II}P\text{-}NO]$, $[Fe^{III}P\text{-}NO]^+$, $[MI\text{-}Fe^{II}P\text{-}NO]$, $[MI\text{-}Fe^{III}P\text{-}NO]^+$ respectively for four coordinated heme, NO ligated and six coordinated heme-NO systems will be used hereafter (P states to porphyrin and MI refers to 5-methyl imidazole).

2. Computational methods

2.1. The heme-model systems

To investigate environment effect on NO binding to ferrous and ferric-heme, we have considered three models:

(i) The iron–porphyrin–NO in five- and six coordinated states.

(ii) Histidine interacted model in five- and six coordinated states from distal position.

(iii) Mono-hydrated systems in five- and six coordinated states (see Fig. 1).

In this regard, the 3D coordinates of the crystal structure of oxyMb at 1.0 Å resolution has been selected as the heme model (PDB ID 1A6M)[23] then O_2 was replaced by NO in the next step, for further studies and to investigate the effect of histidine (HIS64), the side chains of the heme systems were replaced all by hydrogen atoms. We previously showed that this system is a suitable minimal model to investigate binding interactions.[22] Furthermore, following Kepp *et al.*,[24] the distal MI was modeled as a HIS64 (wild type) for the Fe^{II} and Fe^{III} systems. Based on Kepp and Dasmeh,[24] in distal imidazole, the α carbon was replaced by a hydrogen atom and then kept fixed in all geometry optimizations to prevent system deformation and change in system conformation. Also, in line with our previous studies,[22,25] the 5-methyl imidazole (MI) group was considered as the histidine residue in axial position. As shown in Fig. 1, the NO is positioned bent to the Fe^{II} and linear to the Fe^{III} and the methyl-imidazole is placed on the 6th coordinated axial ligand to Fe^{II} and Fe^{III}.

Moreover, the effect of MI as the model of HIS64 on NO, with Fe^{II} and Fe^{III}-porphyrins in 5 and 6 coordinated states in the presence and absence of water molecule with water hydrogen binding role have been also investigated. It is worth mentioning that the most stable spin states have been considered for heme-Fe^{II} and heme-Fe^{III} complexes, namely the doublet state for 5 and 6 coordinated heme-Fe^{II}-NO[18,26] and the singlet state for 5 and 6 coordinated heme-Fe^{III}-NO.[17,18] We have used the deMon2k software[27] in the auxiliary density functional theory (ADFT) framework for geometry optimizations of considered systems. ADFT is a fast and robust method and also computationally cost-effective DFT methodology that resorts to variationally fitted densities to evaluate classical coulombic and exchange-correlation (XC) contributions.[28]

2.2. Methodology: ADFT and geometry optimization

We used OPBE as a XC functional developed by Swart and coworkers,[29] that combines the OPTX exchange functional to the Perdew–Burke–Ernzerhof (PBE) model of electronic correlation. A double zeta valence polarization basis set calibrated for the first row transition metals have been employed for application with generalized gradient approximation (GGA) functionals have been chosen (DZVP-GGA). We have worked with the spin-unrestricted open shell Kohn–Sham (SR UKS) formalism for all calculations. ADFT relied on fitted electronic densities that are expanded on automatically generated auxiliary basis sets. We have considered the GEN-A2, which contains s, p and d auxiliary functions for C, H, and the GEN-A2* auxiliary function sets, that includes, p, d, f, and g auxiliary functions, for Fe, N, and O in NO as a ligand. Moreover, an empirical dispersion energy correction has been used due to the importance of van der Waals interaction between CO and considered systems.[30,31]

To integrate the XC energy and potential, an adaptive grid of fine accuracy has been used (10^{-6} Ha). SCF iterations and geometry optimizations were also performed with convergence criteria of 10^{-7} Ha and 10^{-5} Ha bohr^{-1} respectively (Ha stands for Hartree).

Vibrational frequencies were calculated on the optimized structures at PBE/DZVP/GEN-A2* level of theory. These analyses confirmed that all structures were at their lowest energy state and no imaginary frequencies appeared.

2.3. Binding energy and QTAIM studies

We have determined binding energies of NO to heme (Fe^{II}, Fe^{III}) in the presence and absence of environmental species. As explained above ground state geometry optimizations have been carried out at the OPBE/DZVP-GGA level, and

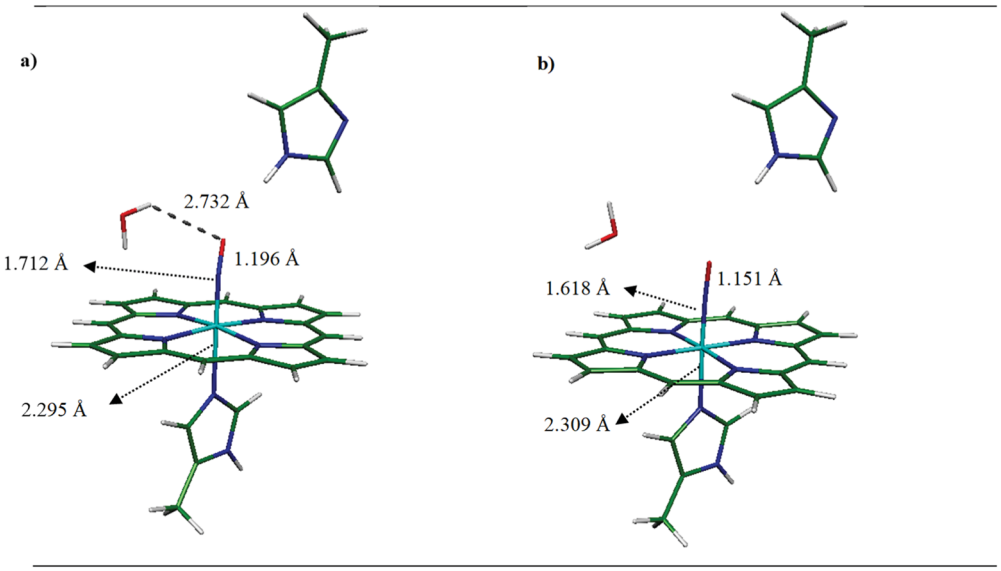

Fig. 1 Optimized structure and model system for (a) [MI-Fe^{II}P-NO···MI] and (b) [MI-Fe^{III}P-NO···MI]$^{+}$ determined at the OPBE/DZVP-GGA/GEN-A2* level of theory.

subsequently, binding energies have been determined in gas phase or in solvent conductor-like polarizable continuum (CPCM) at the B3LYP/def2-TZVP level for all atoms using Gaussian 16 program.[32] CPCM is used to model the solvent effect in quantum chemical calculations, where the solvent is exhibited as a dielectric polarizable continuum and the solute is located inside the molecular shape cavity. The solvent reaction field is described using polarization charges on the cavity surface. The cavity is created by the GEPOL algorithm by a solvent-excluding or solvent-accessible surface.[33] The binding energy for all structures was corrected by basis set superposition error (BSSE) and also the empirical dispersion (DJ). The BSSE was evaluated with the counterpoise methodology of Boys and Beranrdi.[34] Empirical dispersion was added using B3LYP/def2-TZVP/GDBJ (D3 version of Grimme with Becke-Johnson damping factors).[35] Additionally, the binding energy of NO complexation to penta (5) and hexa (6) coordinated of Fe^{II}P and Fe^{III}P were calculated at B3LYP/def2-TZVP level of theory and are compared with the values of binding energy from previous experimental and computational methods[13,36–38] (see Table S1 in ESI File).†

Bader's Quantum Theory of Atoms in Molecules, (QTAIM), analyzes a various interaction of inter- and intramolecular, specially atom–atom interaction *e.g.* covalent bonds, or hydrogen bonds as an intermolecular bonding interactions.[39] In this study, QTAIM has been carried out using AIMAll software.[40]

3. Results and discussions

3.1. Ferrous-heme

3.1.1. Structural parameters. The optimized structures of individual heme and its ligated to NO analogs have been extensively investigated and reported in literature.[9,13,15,16,31,37,38,41,42] We have determined and presented the optimized structures for several [Fe^{II}P-NO] complexes in Fig. 2. As shown, in agreement we previous reports,[14,17,43,44] the NO connects to Fe from N side and the Fe–N–O is bent (~140°). In present work, we disregarded the structural analysis of heme-NO, instead, we have focused on the distal interacted analogues. The ground state of heme-NO complexes is in a doublet spin-state. The NO complexation to [Fe^{II}P] in the free and in presence of the HIS64 (MI) distal group has been presented in Fig. 2, and Table 1. The results indicate that the porphyrin ring in [Fe^{II}P-NO] and [Fe^{II}P-NO···MI] complexes retain their planarity along with slightly out-of-plane doming (0.262–0.268 Å) on Fe atom. Furthermore, in the [Fe^{II}P-NO] complex, the Fe–NO and N–O bond lengths and also the Fe–N–O bond angle have been evaluated to 1.690, 1.183 Å, and 145.3° respectively. The computed Fe–N–O angle (145.3°) in this work agrees well with the crystal structure for the [Fe^{II}-TPP(NO)] (144.4°).[43]

NO complexation patterns to [MI-Fe^{II}P] in free and in presence of MI are collected in Table 1. In six-coordination complexes, the planarity of porphyrin ring is well-preserved. In the 6-coordinated complexes (6C), binding of NO to [MI-Fe^{II}P] complex leads to stability of the Fe–NO interaction and also the *trans*-repulsive effect of the NO ligand on axially coordinated N-donor MI ligand, which induces elongated Fe^{II}–N$_{ax}$ bond length.[16] As a result, the MI in the proximal position is almost displaced and gets away from Fe. Moreover, the Fe–N$_{ax}$ bond length (2.212 and 2.252 Å) are longer than corresponding bonds in the decarboxylase (2.125 Å).

In the [MI-Fe^{II}P-NO] complex, the Fe–NO and N–O bond lengths and also the Fe–N–O bond angle has been evaluated to 1.724, 1.185 Å, and 140.1° respectively. Moreover, the Fe–NO and N–O distances in [MI-Fe^{II}P-NO] complex are longer than the corresponding bond lengths in [Fe^{II}P-NO] complex and the bending of Fe–N–O angle in six coordinated complex (~5°) is

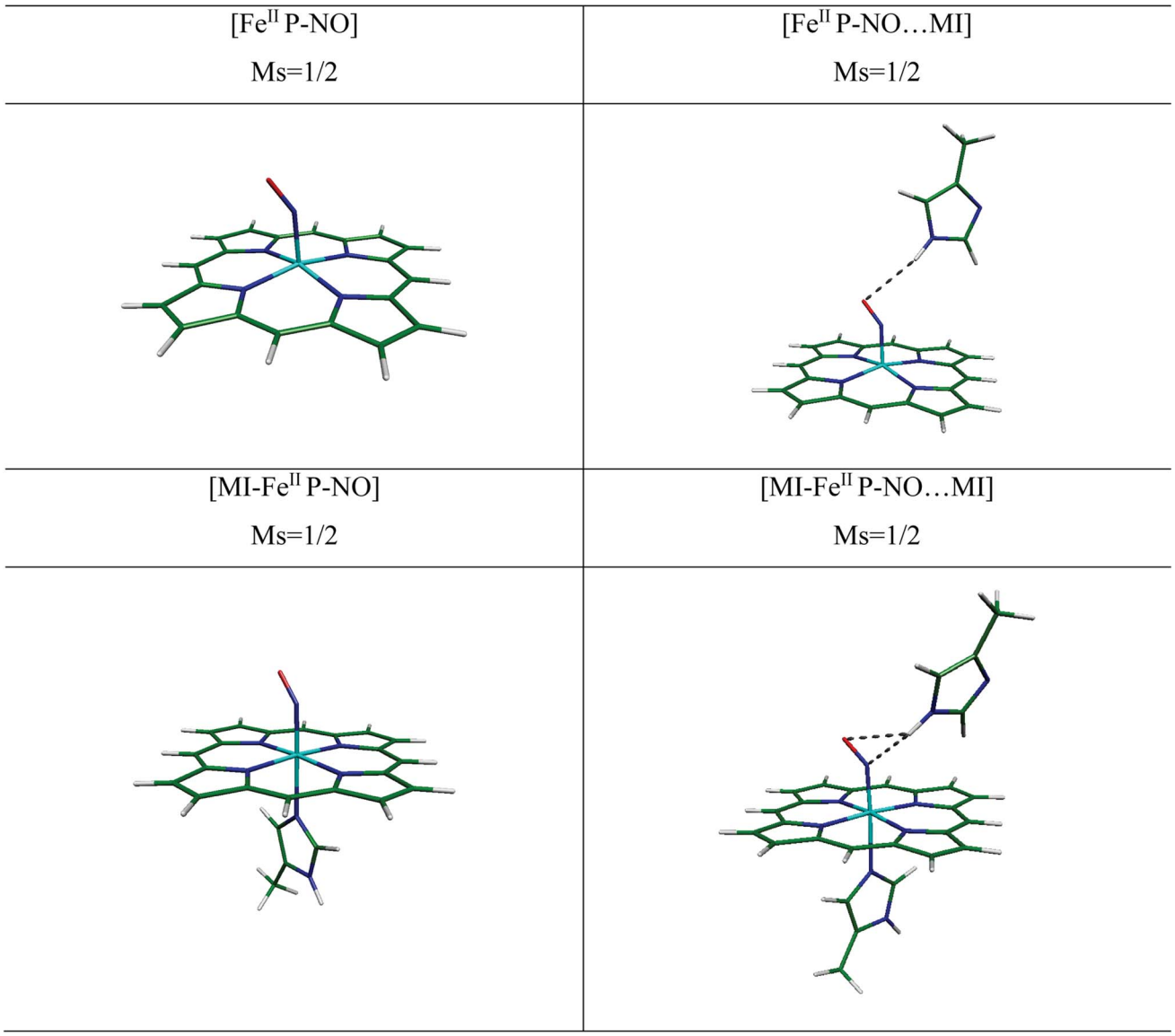

Fig. 2 The optimized structures of complexes of ferrous with NO ligand investigated with/without HIS64 (MI) distal group at the OPTX-PBE/DZVP-GGA/GEN-A2* level of theory. M_s indicates to spin quantum number.

more than the corresponding bond angle in the 5 coordinated complex (5C). Also, the Fe–N–O bond angle (140.1°) is in agreement with experimental X-ray data for [Fe^{II}(TPP)(NO)(1-MeIm)] complex,[44] however the Fe–NO, N–O, and Fe–N_{ax} bond lengths (1.743, 1.144, and 12.180 Å) have been only slightly differed by 0.019, 0.041 and 0.032 Å with [MI-Fe^{II}P-NO] complex in this work. Furthermore, our calculated minimum structural parameters of [MI-Fe^{II}P-NO] are almost in agreement with literature.[14,15] Therefore, the consistency of geometry parameters with experimental results confirms the validity of our theoretical results for the investigation of considered heme models.

In the [MI-Fe^{II}P-NO···MI] complex (Fig. 2), in presence of distal MI the Fe–NO bond has been predicted to be slightly shortened (from 1.724 Å to 1.716 Å), and other bond lengths (N–O, Fe–N_{eq}, and Fe–N_{ax}) exhibit no significant change. Furthermore, the calculated Fe–NO and N–O bond lengths of 1.716 and 1.191 Å, are comparable with the corresponding experimental X-ray values of 1.889 and 1.154 Å (ref. 11) respectively which are also in line with Liao's report.[15]

Moreover, an inspection of the vibrational frequency of normal modes in [MI-Fe^{II}P-NO], compared to [MI-Fe^{II}P-NO··· MI] exhibits that the vibrational frequency of Fe–NO stretching-mode is 624 cm^{-1} (in the absence of distal MI) and 634 cm^{-1} (in presence of MI). In addition, in the [MI-Fe^{II}P-NO···MI] complex, the $N_{(NO)}$···$HN_{(MI)}$ and $O_{(NO)}$···$HN_{(MI)}$ distances have been determined to be 2.693 and 3.013 Å (see Table 1) which indicate to increase in π-back-donation from the occupied dπ (d_{xz} and d_{yz}) orbitals of iron to unoccupied π*–NO orbitals. Since slight alteration in geometry parameters and vibrational frequency has been predicted, it could be concluded that distal MI (in absence of hydration) only slightly affects the Fe^{II}–NO

Table 1 Selected optimized geometry parameters (bond lengths in Å and bond angles in degree) for most stable spin states of the relevant ferrous heme systems ligated to NO and in presence of distal moieties

Complex	M_s	Fe–N_{NO} (Å)	N–O (Å)	Fe-N_{ax} (Å)	Doming	∠FeNO	O (N)···H_{distal} (Å)	ν(Fe–N) cm^{-1}	ν(N–O) cm^{-1}
[Fe^{II}P-NO]	2	1.690	1.183	—	0.262	145.294	—	634.1	1779.90
Experiment[41]		1.717	1.122			144.4			
Calculated[37]		1.69	1.19			146			
[Fe^{II}P-NO···MI]	2	1.690	1.183	—	0.268	144.611	3.415 (O···H) 2.974 (N···H)	632.9	1760.30
[MI-Fe^{II}P]	5	—	—	2.125	−0.252	—	—	—	—
Exp.[23]				2.141	−0.365				
[MI-Fe^{II}P-NO]	2	1.724	1.185	2.212	0.082	140.1	—	624.0	1765.8
Experiment[44]		1.743	1.144	2.180		142.2			
Calculated[37]		1.720	1.200	2.220		138.0			
[MI-Fe^{II}P-NO···MI]	2	1.716	1.191	2.252	0.083	140.19	2.693 (N···H)	634.0	1732.7
Calculated[15]		1.728	1.195	2.182	−0.071	140.90	3.013 (O···H) 3.06 (O···H) 2.357 (N···H)		
[Fe^{II}P-NO]···H_2O	2	1.684	1.186	—	0.268	145.110	2.737 (O···H_w)	644.4	1765.40
[Fe^{II}P-NO···MI]···H_2O	2	1.681	1.192	—	0.264	143.894	2.590 (O···H_{MI}) 2.511(O···H_w)	647.2	1741.10
[MI-Fe^{II}P]···H_2O	5	—	—	2.115	−0.232	—	—	—	—
[MI-Fe^{II}P-NO]···H_2O	2	1.710	1.192	2.304	0.074	140.126	2.903 (N···H_w) 2.687 (O···H_w)	652.9	1727.2
[MI-Fe^{II}P-NO···MI]···H_2O	2	1.712	1.196	2.295	0.108	139.232	3.090 (O···H) 3.045 (N···H_w) 2.732 (O···H_w)	636.7	1727.2

interaction in heme system. In comparison NO ligation of heme in Mb, the NO interaction with cytochrome c' (AXCP) has been investigated by Marti *et al.*[45] and the optimized parameters have been reported there. In the presence of distal group (LEU16) of AXCP, the Fe–NO, N–O and Fe–N_{ax} bonds have been reported to 1.74, 1.21, and 2.33 Å (in protein media) by QM/MM and also 1.75, 1.21, and 2.24 Å (in gas phase) by QM method. In the ligation of NO to AXCP, due to the negative NO trans effect, the Fe–N_{ax} has been reported to be weakened. In other work by Marti (2008),[46] the NO interaction with HB has been investigated by molecular dynamics (MD) simulations. The results demonstrated that due to trans effect of $N_{(NO)}$–Fe–N_{ax}, the Fe–N_{ax} is weakened. These results are in agreement with the optimized geometry parameters of [MI-Fe^{II}P-NO···MI] in our work.

3.1.2. Water hydrogen bonding. Owing to the importance of solvation effect on binding of biological ligands and more especially in heme systems,[24] we have investigated the explicit inclusion of a water molecule on binding of NO to heme and also the bulk model (with CPCM methodology). The direct molecular interactions could not be studied in implicit model; thus we have investigated this subject based on the water hydrogen bonding to follow accurately the effect of H-bonding. We report the optimized geometry parameters of microhydrated systems in Table 1. The water molecule interacts with NO *via* a hydrogen bond. As shown in Table 1, water hydrogen binding affects the geometrical parameters of [Fe^{II}P-NO] complex, the Fe–NO bond length has been slightly shortened by ∼0.006 Å (from 1.690 Å to 1.684 Å). In this system, a hydrogen bond is formed between H_2O and NO. Also, the vibrational frequencies of ν(Fe–NO) have been slightly altered from 634.1 cm^{-1} to 644.4 cm^{-1} respectively in the absence- and presence of water molecule ($\Delta\nu = 10.4$ cm^{-1}). Consequently, the water hydrogen bonding has slightly affected the complexation of NO to five coordinated ferrous complexes. By comparing individual [MI-Fe^{II}P-NO] complex with mono-hydrated [MI-Fe^{II}P-NO]···H_2O, the slight change on Fe–NO (1.710 Å) and N–O (1.192 Å) bond distances have been predicted. Moreover, the HOH···ON hydrogen bond leads to a change in the vibrational frequencies of Fe–NO and N–O (from 624.0 cm^{-1} in [MI-Fe^{II}P-NO] complex to 652.9 cm^{-1} in [MI-Fe^{II}P-NO]···H_2O complex by 29 cm^{-1}). As shown, water hydrogen bonding affects the geometrical parameters of [MI-Fe^{II}P-NO···MI] complex, the Fe–NO bond has been slightly shortened by ∼0.004 Å (from 1.716 Å to 1.712 Å). As a consequence, the MI distal group, as well as water H-bond, significantly affect the interaction of NO to six coordinated ferrous complexes (see Table 1, and also ESI file for more information regarding the optimized geometry parameters).†

3.1.3. Interaction energies of NO-heme. Binding energies, ΔE_c corrected by BSSE and empirical dispersion, has been calculated at B3LYP/def2-TZVP level of theory in the gas phase as well as solvent medium ($\varepsilon = 78$) using the following equations:

$$\Delta E_{binding} = E_{[Fe^{II}P\text{-}NO\cdots MI]}(\mathrm{LS}, S = 1/2) - (E_{[Fe^{II}P\cdots MI]}(\mathrm{HS}, S = 1) + E_{[NO]}(S = 1/2)) \quad (1)$$

$$\Delta E_{binding} = E_{[MI\text{-}Fe^{II}P\text{-}NO\cdots MI]}(\mathrm{LS}, S = 1/2) - (E_{[MI\text{-}Fe^{II}P\cdots MI]}(\mathrm{HS}, S = 2) + E_{[NO]}(S = 1/2)) \quad (2)$$

where LS and HS are low spin and high spin. The binding energy reflects the energy differences arising from the complexation of distal residue to 5 and six coordinated systems

in the absence or presence of water molecules. We have tabulated these results in Tables 2 (and S3 in ESI file).†

As presented in Table 2, The binding energy of [Fe^{II}P-NO] has been reported experimentally to be −26.6 and −28.9 kcal mol^{-1} ([Fe^{II}-Tpyr-PH_2-NO]$^{2+}$) by Chen *et al.*[47]

Furthermore, NO-binding energy to ferrous heme has been determined theoretically by several groups[15,37,38] being reported within the broad range of –(5.5–32.0) kcal mol^{-1} based on the different theoretical levels. In the present study, the binding energy for heme-NO has been determined to −16.6 kcal mol^{-1} at B3LYP/def2-TZVP level of theory. It can be concluded that the binding energy values are quite sensitive to the choice of DFT method, nevertheless, the selected theoretical model of this work has been previously examined for heme systems and gave reliable results.[22,25]

In the presence of the MI in distal position (*i.e.*, in [Fe^{II}P-NO⋯MI] complex), we have determined the binding energy of NO to 4C heme-NO to −16.5 and −14.8 kcal mol^{-1} in the gas phase and implicit solvent medium respectively. In the 6-coordinated [MI-Fe^{II}P-NO] complex, the binding energy has been determined to −17.9 kcal mol^{-1}. This is while the experimental binding energy of NO in [MI-Fe^{II}P-NO] complex has been reported to −22.8 kcal mol^{-1} by Olson[10] and Springer.[48] Nevertheless, the corresponding theoretical value has been reported to lie within the range of –(12.45–36.0) kcal mol^{-1} by different theoretical groups.[13,37,38,49,50] Thus, our theoretical result (−16.5 kcal mol^{-1}) is in good agreement with experimental- and previous theoretical reports as well.

Moreover, in Table 2, water H-bond effect, in addition to distal group, has been presented. In the [Fe^{II}P-NO]⋯H_2O complex, the formation of the HOH⋯ON hydrogen bond, results in a slight shortening in the Fe–NO bond length and increases the ν(Fe–NO) vibrational frequency. The binding energies are determined to −17.2 kcal mol^{-1}. Moreover, in the [Fe^{II}P-NO⋯MI]⋯H_2O complex, the interaction of NO to [MI-Fe^{II}P⋯MI]⋯H_2O is strengthened by the formation a hydrogen bond.

3.1.4. QTAIM results: Fe–NO bond analysis. In order to further characterize NO ligation, we have carried out the QTAIM analyses, which rely on topological analyses of electron-density distribution $\rho(r)$.[39] Within the QTAIM framework, chemical bonding can be assessed with regard to features of the bond critical points (BCPs) in $\rho(r)$. Fig. 3 shows the molecular graph of [MI-Fe^{II}P-NO⋯MI] and [MI-Fe^{II}P-NO⋯MI]⋯H_2O complex. The classical covalent or coordination bonds are shown as solid lines, and closed-shell intramolecular interactions are shown as dashed lines for (i) Fe–NO bond, (ii) O⋯H_{MI}, N⋯H_{MI} and O⋯H_w interactions in these complexes. Topological properties at BCPs for Fe–NO, O⋯HMI (N⋯H_{MI}) and O⋯H_w bonds in five coordinated and six coordinated complexes in free and presence of MI as a distal and also in microhydrated systems are collected in Table S4 (in ESI file).†

To simplify, we follow our comparative studies to investigate the variation in topological properties with a change in the interatomic distances, d(Fe–NO). Concerning the NO–Fe bond, the ρ_{BCP} is significantly large (0.169 a.u. < $\rho(r)$ < 0.194 a.u.) and $\nabla^2\rho_{BCP}$ is positive (0.784 a.u. < $\nabla^2\rho(r)$ < 0.830 a.u.) indicating a "partially covalent" character of the coordination bonds.[51] Furthermore, the values of local electron potential energy density, $V(r)$ (−0.339 a.u. < $V(r)$ < −0.387 a.u.), is larger than the local electron kinetic energy density $G(r)$ (0.268 a.u. < $G(r)$ < 0.289 a.u.). The $|V(r)|/G(r)$ ratio is another useful parameter, the 1 < $|V(r)|/G(r)$ < 1.325 and $|V(r)|/G(r)$ < 1 is characteristic of an ionic interaction and $|V(r)|/G(r)$ > 2 indicates to a pure covalent bond. Therefore, our QTAIM analysis indicates that the Fe–NO bond is not only a pure covalent bond but also it has both the ionic/covalent characters.

Moreover, from Table S3,† it is seen that with shortening Fe–NO bond length in [Fe^{II}P-NO⋯MI]⋯H_2O compared to its individual analogue (([MI-Fe^{II}P-NO]) to [MI-Fe^{II}P NO⋯MI]⋯H_2O) the ρ_{BCP} increases and also V_{BCP} becomes more negative when d(Fe–NO) decreases.

Due to this fact that the BCP with 0.002 < $\rho(r)$ < 0.035, $\nabla^2\rho(r)$ > 0, $|V(r)|/G(r)$ < 1 and $H(r)$ > 0 is indicative of the presence of closed-shell (non-covalent bond such as hydrogen bond, van der walls, ionic interaction).[39,51] In the distal interacted [Fe^{II}P-NO⋯MI] complex, the ρ_{BCP} and $\nabla^2\rho_{BCP}$ at BCP of N⋯H_{MI} bond are calculated to be 0.006 and 0.021, respectively. These values are both in the range of hydrogen bond interaction. Also, in monohydrated [Fe^{II}P-NO⋯MI]⋯H_2O complexes, the ρ_{BCP} and $\nabla^2\rho_{BCP}$ values at BCP of O⋯H_w and O⋯H_{MI} bonds are within 0.004–0.006 and 0.014 < $\nabla^2\rho_{BCP}$ < 0.023 which are both relatively significant, being in the range of strong hydrogen bonds. In the six coordinated complex of [MI-Fe^{II}P-NO]⋯H_2O, the ρ_{BCP} and $\nabla^2\rho_{BCP}$ values at BCP of O⋯H_w bond are evaluated to 0.005 a.u. and 0.017 a.u. respectively, confirming the existence of a hydrogen bond between H (H_2O)⋯O (NO).

Due to the large ρ_{BCP} (0.169 a.u. < $\rho(r)$ < 0.194 a.u.) and positive $\nabla^2\rho_{BCP}$ (0.784 a.u. < $\nabla^2\rho(r)$ < 0.830 a.u.), it can be concluded that the Fe^{II}–NO bond has an ionic-covalent property.

Table 2 Binding energy of NO/heme ligation in different conditions determined at B3LYP/def2-TZVP level of theory

Complex	ΔE (kcal mol^{-1}) (gas)	ΔE (kcal mol^{-1}) (solvent)
[Fe^{II}P-NO]	−16.6	−15.8
Experiment:[47] −26.6 ± 0.7		
Calculated:[38] −27.5		
[Fe^{II}P-NO⋯MI]	−16.5	−14.8
[MI-Fe^{II}P-NO]	−17.9	−16.9
Calculated:[49] −16.3		
[MI-Fe^{II}P-NO⋯MI]	−19.1	−16.7
Experiment[38] (Mb-NO): −22.8		
[Fe^{II}P-NO]⋯H_2O	−17.2	−14.1
[Fe^{II}P-NO⋯MI]⋯H_2O	−19.9	−17.0
[MI-Fe^{II}P-NO]⋯H_2O	−19.8	−16.8
[MI-Fe^{II}P-NO⋯MI]⋯H_2O	−19.6	−16.3

3.2. Ferric-heme

3.2.1. Structural parameters. The geometries of [Fe^{III}P]$^+$ and [MI-Fe^{III}P]$^+$ with NO in presence of HIS64 (MI) as a distal

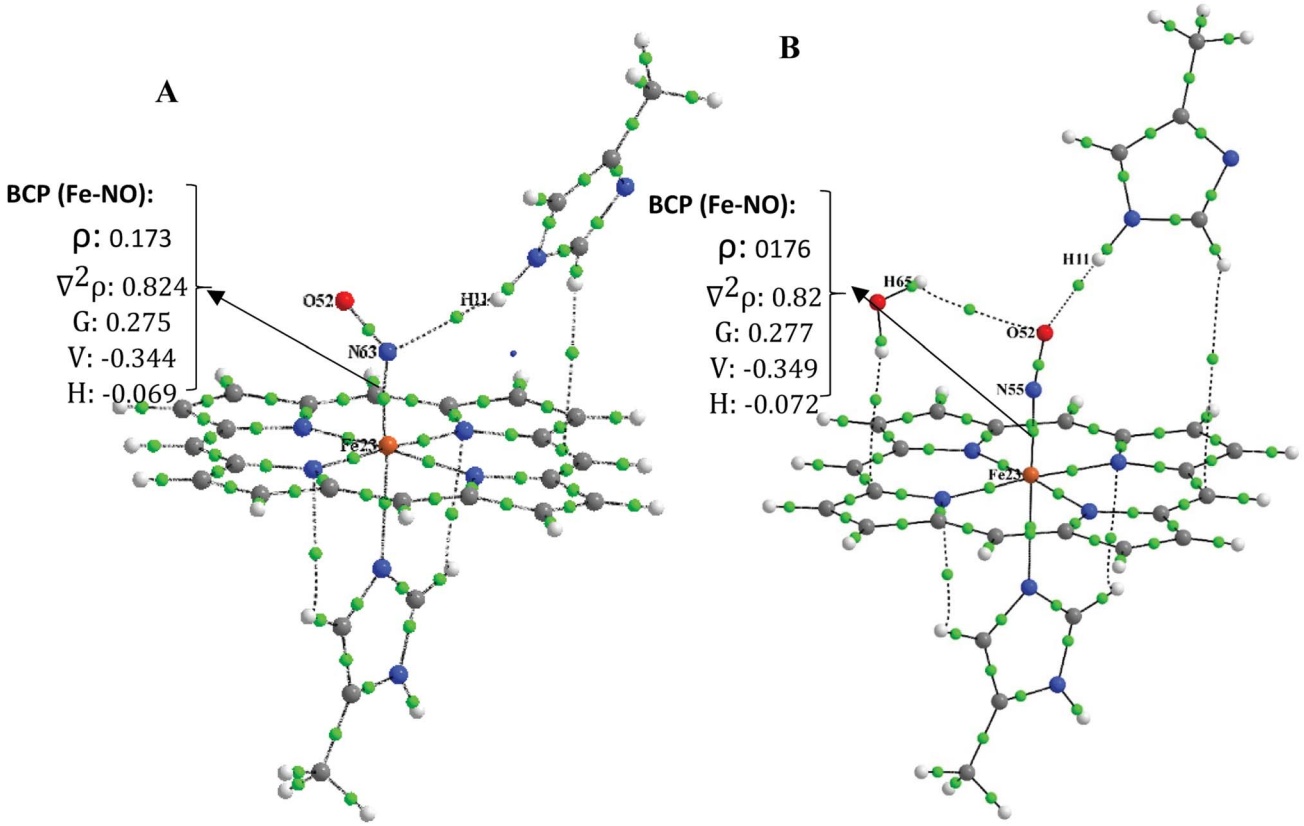

Fig. 3 The QTAIM molecule graph of (A) [MI-Fe^{II}P-NO···MI] complex, (B) [MI-Fe^{II}P-NO···MI]···H_2O.

group without and with water were optimized. The optimized geometry parameters are tabulated in Table 3 and their structures are indicated in Fig. 4 and also ESI file.† The ground state of these complexes are low spin ($S = 0$). According to Praneeth *et al.*, in Ferric heme, the Fe^{III}–NO interaction could be described as Fe^{II}–NO$^+$, being isoelectronic with Fe^{II}–CO complexes. This electronic structure corresponds to oxidation of NO upon binding to Fe^{III} and thus shows a linear Fe–N–O angle.[17]

Table 3 Selected optimized geometry parameters (band lengths, Å and bond angles, degree) for most stable spin states of the relevant ferric heme systems ligated to CO and in presence of MI (HIS64) as a distal moiety at the OPTX-PBE/DZVP-GGA/GEN-A2* level of theory. The N_{ax} are the coordinated MI nitrogen, respectively. The vibrational frequencies have been calculated at PBE/DZVP/GEN-A2* level of theory

Complex	M_s	Fe–N_{NO} (Å)	N–O (Å)	Fe-N_{ax} (Å)	Doming[a]	∠FeNO	O (N)···H_{distal} (Å)	ν(Fe–N) cm^{-1}	ν(N–O) cm^{-1}
[Fe^{III}P-NO]$^+$	1	1.599	1.159	—	0.335	179.955	—	435.6	2002.9
Calculated[55]		1.614	1.145		—	180.0			
[Fe^{III}P-NO···MI]$^+$	1	1.605	1.164	—	0.314	172.384	2.900	425.8	1961.20
[MI-Fe^{III}P]$^+$	6	—	—	2.075	−0.394	—	—	—	—
Calculated[22]				2.100	−0.430				
[MI-Fe^{III}P-NO]$^+$	1	1.620	1.150	2.017	0.066	179.300	—	627.1	2027.00
Experiment[b,53]		1.628	1.148	1.973	—	176.300			
[MI-Fe^{III}P-NO···MI]$^+$	1	1.618	1.151	2.039	0.035	179.394	3.575	629.3	2022.10
Calculated[56]		1.650	1.130	2.020		175.80	—		
[Fe^{III}P-NO]$^+$···H_2O	1	1.600	1.156	—	0.323	179.440	3.201 (O···O)	433.5	2012.80
[Fe^{III}P-NO···MI]$^+$···H_2O	1	1.606	1.161	—	0.325	166.543	3.298 (O···O) 2.607 (O···H)	417.0	1966.50
[MI-Fe^{III}P]$^+$···H_2O	6	—	—	2.066	0.376	—	—	—	—
[MI-Fe^{III}P-NO]$^+$···H_2O	1	1.618	1.146	2.043	0.034	179.416	3.068 (O···O)	630.8	2060.30
[MI-Fe^{III}P-NO···MI]$^+$···H_2O	1	1.620	1.147	2.042	0.036	176.979	3.463(O···H) 3.070 (O···O)	621.8	2041.50

[a] Displacement of the Fe from the porphyrin and heme plane that is defined as doming. [b] [Fe^{III}(NO)(TPP)]ClO_4.

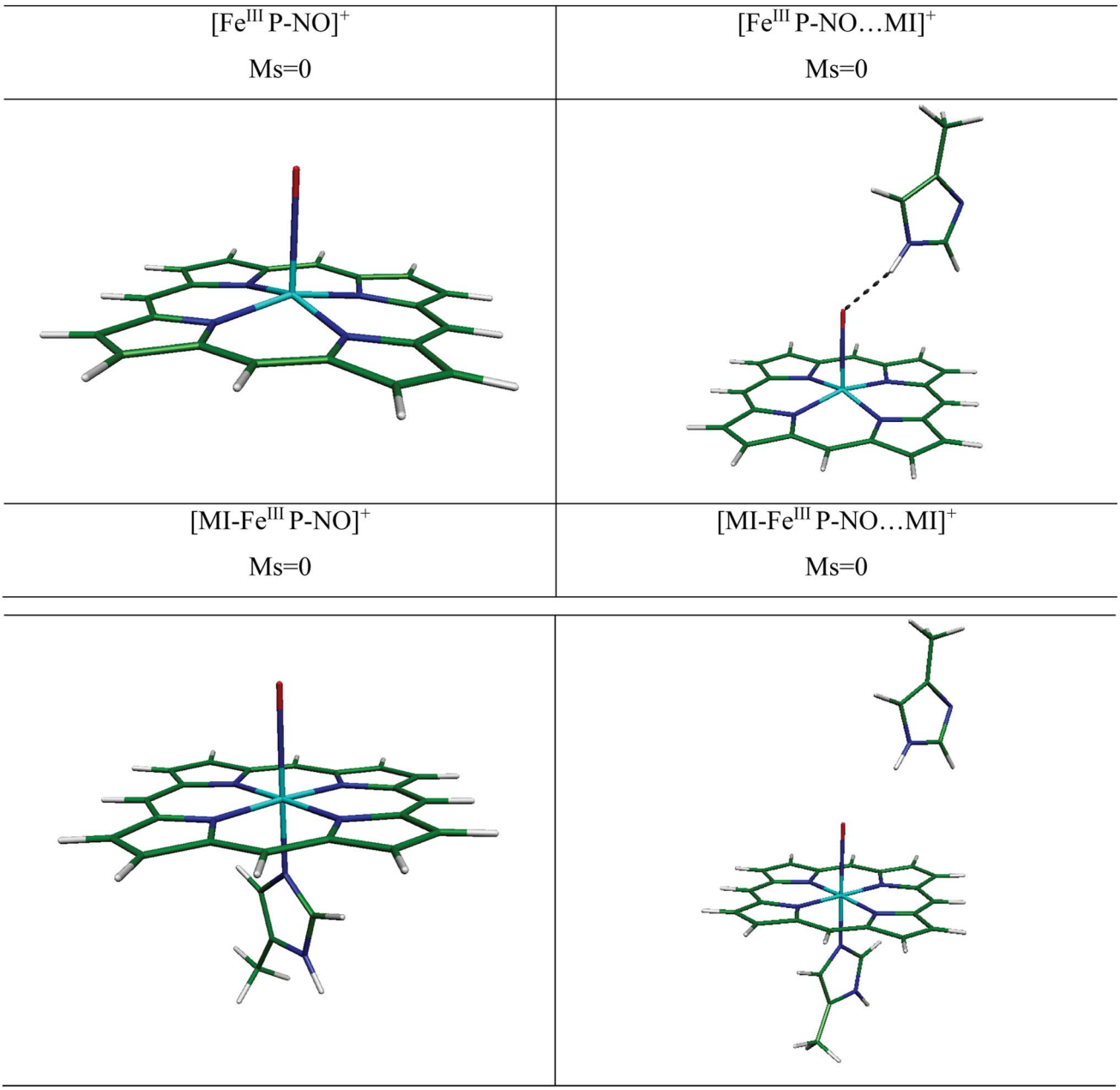

Fig. 4 The optimized structures of complexes of ferric with NO ligand investigated with/without HIS64 (MI) distal group at the OPTX-PBE/DZVP-GGA/GEN-A2* level of theory. M_s indicates to spin quantum number.

(i) In the bare and distal interacted $[Fe^{III}P\text{-}NO]^+$ and $[MI\text{-}Fe^{III}P\text{-}NO]^+$. We have investigated the NO ligation to $[Fe^{III}P]^+$ in free and presence of distal MI. We have presented the optimized structures for several $[Fe^{III}P\text{-}NO]^+$ complexes in Fig. 4. In the presence of distal MI, the planarity of porphyrin ring in the $[Fe^{III}P\text{-}NO]^+$ and $[Fe^{III}P\text{-}NO\cdots MI]^+$ complexes have been significantly preserved and the out-of-plane distortion of Fe from the porphyrin plane (doming) is in the range of 0.314–0.335 Å.

The experimental and theoretical studies of geometry and electronic structure of ferric heme-NO have been investigated by several groups.[22,52,53] The experimental values of Fe–NO and N–O bond lengths have been reported to be in the range of 1.640–1.644 Å and 1.110–1.153 Å, respectively.[52,53] In the $[Fe^{III}P\text{-}NO\cdots MI]^+$ complex, in the presence of distal group, the Fe–NO bond length slightly elongates (0.006 Å), the Fe^{III} out-of-plane doming (0.021 Å) and Fe–N–O angle (7.6°) decrease, compared to its individual analogue. Furthermore, the vibrational frequencies of ν(Fe–NO) has been poorly changed from 435.6 cm^{-1} to 425.8 cm^{-1} in the presence of MI (9.8 cm^{-1}). Consequently, it could be concluded that the distal MI residue has a negligible effect on NO bonding to 5C ferric-heme.

We have also determined the optimized structure of the 6C $[MI\text{-}Fe^{III}P\text{-}NO]^+$ systems, in the presence and absence of distal MI (see Table 3). In $[MI\text{-}Fe^{III}P\text{-}NO]^+$ and $[MI\text{-}Fe^{III}P\text{-}NO\cdots MI]^+$,

the planarity of porphyrin ring is preserved. The strong π-back bonding and weak σ-bond explain the short Fe–NO bond in [MI-Fe^{III}P-NO]$^+$ and insignificant *trans*-effect of NO in ligation of NO with ferric-heme.[17,18,54] In the [MI-Fe^{III}P-NO]$^+$ complex, the Fe–NO and N–O are determined to be 1.620 and 1.150 Å, respectively. Also, the Fe–N_{ax} bond length and Fe–N–O angle are 2.017 Å and 179.30°. In the [Fe(TPP)(NO)(MI)]PO_2F_2 complexes,[53] the Fe–NO bond lengths have been evaluated in the range 1.628 and N–O 1.148. Å, in agreement with the obtained structural parameters (Fe–NO: 1.620 Å, N–O 1.150 Å). Other calculated structural parameters of [MI-Fe^{III}P-NO]$^+$ contain the Fe–N_{ax} (2.00 Å) and Fe–N–O angle (179.300°) and the vibrational frequency of ν(Fe–NO) is calculated 627.10 cm^{-1}. In the [MI-Fe^{III}P-NO···MI]$^+$ complex, the calculated values of Fe–NO and N–O bond lengths are 1.618 and 1.151 Å being comparable with the corresponding computational results of 1.650 and 1.130 Å. In the presence of distal MI residue, the Fe–NO has been predicted to be slightly shortened (from 1.620 Å to 1.614 Å). However, since the alteration in geometry parameters and vibrational frequency is poorly significant, it could be concluded that distal MI has not a significant alteration effect on the Fe^{III}–NO bonding in heme system. We will investigate this issue in the next sections by considering binding energy values and QTAIM results.

(ii) Water H-bond effect. Due to the significant solvent effect on NO binding, in this section we have investigated the effect of explicit water on NO ligation of ferric-heme system. The optimized geometry parameters of hydrated systems have been tabulated in Table 3. Also, the optimized structures have been presented in Fig. S2 in ESI file.† As shown, water H-bond affects the geometry parameters of [Fe^{III}P-NO···MI]$^+$ complex, the Fe^{III} out-of-plane doming (0.011 Å) increases, the Fe–N–O angle decreases from 172.82° in [Fe^{III}P-NO···MI]$^+$ complex to 166.54° in [Fe^{III}P-NO···MI]$^+$···H_2O system. In this system, an H-bond between distal MI and $O_{(NO)}$ have been predicted to form. Thus, the vibrational frequencies of ν(Fe–NO) has been red-shifted from 425.8 cm^{-1} in the absence of water molecule to 417.0 cm^{-1} in the presence of that (~8.8 cm^{-1}). Consequently, the distal MI and also water H-bond have no significant effect on binding of NO to 5C ferric heme.

By comparing individual [MI-Fe^{III}P-NO···MI]$^+$ complex with water H-bond [MI-Fe^{III}P-NO···MI]$^+$···H_2O analogue, poorly change on Fe–NO (1.620 Å) and N–O (1.147 Å) bond distances have been predicted. Also, the vibrational frequencies of Fe–NO and N–O have been slightly changed (from 629.3 cm^{-1} in [MI-Fe^{III}P-NO···MI]$^+$ complex to 621.8 cm^{-1} in [MI-Fe^{III}P-NO···MI]$^+$···H_2O complex (by 7.5 cm^{-1})) and there is no hydrogen bond between H (distal MI) and H_2O with NO. We will more investigate the distal histidine microhydration effects on binding energy of NO to ferric heme in the next sections.

Additionally, more details of optimized geometry parameters and *XYZ* coordinates can be found in ESI file (see Table 3, Fig. 3, S2 and Table S6 in ESI file).†

3.2.2. The interaction energies of NO and ferric-heme. As presented in Tables S4 and S5 (more details) in ESI file,† the ΔE_c in free and presence of distal MI group have been calculated at B3LYP/def2-TZVP level of theory for interaction of NO unit to 4C and 5C of ferric-porphyrin systems ([Fe^{III}P]$^+$ and [MI-Fe^{III}P]$^+$) in the same trend as we already discussed in the previous section (eqn (3) and (4)).

$$\Delta E_{binding} = E_{[Fe^{III}P\text{-}NO\cdots MI]^+}\,(LS,\ S=0) - (E_{[Fe^{III}P\cdots MI]^+}\,(HS,\ S=3/2) + E_{[NO]}\,(S=1/2)) \quad (3)$$

$$\Delta E_{binding} = E_{[MI\text{-}Fe^{III}P\text{-}NO\cdots MI]^+}\,(LS,\ S=0) - (E_{[MI\text{-}Fe^{III}P\cdots MI]^+}\,(HS,\ S=5/2) + E_{[NO]}\,(S=1/2)) \quad (4)$$

For [Fe^{III}P-NO]$^+$ complex, there is π-back bonding between a single two-electron low-spin Fe^{III} dπ (d_{xz}, d_{yz}) orbital and unoccupied NO π* orbital. Furthermore, the other dπ orbital is formed between unoccupied Fe^{III} dπ (d_{xz}, d_{yz}) orbital and half-filled NO π* orbital, and thus a more covalent bond with the lone π*-electron in the HOMO of NO can be organized.[55] As detailed in Table 4, the [Fe^{III}-heme-NO]$^+$ binding energy has been reported experimentally to be −24.88 ± 0.71 kcal mol^{-1} in gas phase[22] and −34.4 kcal mol^{-1} based on the CPMD (Car–Parrinello Molecular Dynamics) theoretical model.[57] We have determined the binding energy for [Fe^{III}P-NO]$^+$ to −11.2 kcal mol^{-1} at B3LYP/def2-TZVP level of theory.

Moreover, the increasing of Fe–NO bond length in [Fe^{III}P-NO···MI]$^+$, from 1.599 Å into 1.605 Å in the presence of MI distal position is in line with decreasing of the calculated binding energy from −11.2 kcal mol^{-1} to −8.0 kcal mol^{-1}. In [Fe^{III}P-NO]$^+$···H_2O complex, in the presence of water molecule, the calculated binding energy has diminished from −11.2 kcal mol^{-1} to −8.1 kcal mol^{-1} while there is a slight alteration compared to [Fe^{III}P-NO···MI]$^+$ (1.605 Å), but the binding energy has been decreased from −8.0 kcal mol^{-1} to −4.9 kcal mol^{-1}.

In the 6 coordinated [MI-Fe^{III}P-NO]$^+$ complex, we have determined the binding energy of NO to −12.3 kcal mol^{-1} in gas phase and −10.1 kcal mol^{-1} in solvent medium. The result of binding energy is in good agreement with computational binding energy (−12.3 kcal mol^{-1} at BP86/TZVP level of theory)

Table 4 Binding energy without/with distal group for Ferric complexes in free and presence of water distal molecule at B3LYP/def2-TZVP level of theory

Complex	ΔE (kcal mol^{-1}) (gas)	ΔE (kcal mol^{-1}) (solvent)
Ferric-heme		
[Fe^{III}P-NO]$^+$	−11.2	−4.2
Experiment:[47] −24.88 ± 0.71		
[Fe^{III}P-NO···MI]$^+$	−8.0	0.5
[MI-Fe^{III}P-NO]$^+$	−12.3	−10.1
Calculated:[17] −12.8		
Calculated:[17] −12.3		
[MI-Fe^{III}P-NO···MI]$^+$	−13.3	−7.2
Ferric-heme (water H-bond effect)		
[Fe^{III}P-NO]$^+$···H_2O	−8.1	−0.7
[Fe^{III}P-NO···MI]$^+$···H_2O	−4.9	2.6
[MI-Fe^{III}P-NO]$^+$···H_2O	−13.1	−8.9
[MI-Fe^{III}P-NO···MI]$^+$···H_2O	−11.2	−6.3

for $[Fe^{III}(P)(MI)(NO)]^+$ in LS state.[17] In presence of distal MI, the Fe–NO bond changes from 1.620 Å ($[MI\text{-}Fe^{III}P\text{-}NO]^+$) to 1.618 Å ($[MI\text{-}Fe^{III}P\text{-}NO\cdots MI]^+$ complex), and the NO binding energy has been determined to −13.3 kcal mol^{-1}. The results indicate that the distal MI group slightly stabilizes the ligation of NO to 6C ferric-heme (∼1.0 kcal mol^{-1}).

Moreover, insertion of a water molecule close to NO in ferric-heme results to no significant alteration in the Fe^{III}–NO bond length. In $[MI\text{-}Fe^{III}P\text{-}NO]^+\cdots H_2O$ complex, the Fe–NO bond is determined to be 1.618 Å, being similar to that of $[MI\text{-}Fe^{III}P\text{-}NO]^+$ complex. Furthermore, in $[MI\text{-}Fe^{III}P\text{-}NO\cdots MI]^+\cdots H_2O$ complex, a small increase in Fe–NO bond distance (from 1.618 to 1.620 Å) results in the slight decrease of the binding energy from −13.3 kcal mol^{-1} (in absence of water molecule) to −11.2 kcal mol^{-1} (in presence of water molecule). As a result, the MI as a distal group slightly stabilizes the interaction of NO ligand to 6C ferric-heme while no significant change has been predicted to take place in the 5C system.

3.3. QTAIM results: Fe–NO bond analysis

3.3.1. Ferric-heme. As presented in Table S4,† to facilitate analysis, the alteration in topological properties with a change in the interatomic distances, d(Fe–NO) has been investigated. The correlations for ρ_{BCP}, and V_{BCP}, G_{BCP}, H_{BCP}, and $|V_{BCP}|/G_{BCP}$ are presented in Fig. S2 of ESI file.† Due to no alteration the bond width of Fe–NO from $[MI\text{-}Fe^{III}P\text{-}NO]^+$ to $[MI\text{-}Fe^{III}P\text{-}NO\cdots MI]^+\cdots H_2O$, the ρ_{BCP}, V_{BCP} and $V(r)/G(r)$ ratio have been slightly changed. In summary, from the QTAIM results, it could be remarked that:

(i) In the 6C ferric-heme complexes, due to the relatively large ρ_{BCP} ($0.197 < \rho(r) < 0.202$ a.u.) and positive $\nabla^2\rho_{BCP}$ (1.406 a.u. $< \nabla^2\rho(r) < 1.445$ a.u.), it can be concluded that the Fe^{III}–NO bond has a polar-covalent property.

(ii) In the 5 and 6C ferric-heme complexes, when both of the MI and H_2O have been considered, the ρ_{BCP} and $\nabla^2\rho_{BCP}$ values at BCP of Fe^{III}–NO bond in ligation of NO to ferric heme only slightly change (0.003–0.005 a.u. for ρBCP) and (0.039–0.118 au for $\nabla^2\rho_{BCP}$).

It is worth noting that the Fe^{III}–NO bond in the 5 and 6C ferric-heme complexes is not a pure covalent bond, instead it has both the ionic and covalent characters.[51] As a consequence, in both 5C and 6C complexes, these results are in well agreement with calculated binding energy values and it seems that the distal MI and water do have a slight effect on strengthening of the NO to ferric heme.

4. Conclusion

Density functional theory has been employed to investigate the effect of distal histidine, water hydrogen bond, and bulk solvent model on the interaction of NO with ferrous and ferric-heme. It has been predicted that water hydrogen bond and distal histidine stabilize NO binding by ∼2.7 kcal mol^{-1} in the 6-coordinated ferrous heme-NO system $[MI\text{-}Fe^{II}P\text{-}NO]$. The results exhibit a synergic effect of water and distal MI interactions on the stabilization of NO–Fe^{II} bond in ferrous heme system, since of the formation of strong hydrogen bonds. This is while the distal MI and water exhibit a less pronounced effect on stabilization of Fe^{III}–NO interaction in ferric heme.

In addition, we have investigated the Fe–NO bond nature based on the Quantum Theory of Atom in Molecule (QTAIM). It has been shown that the Fe–NO bond has partially ionic nature in addition to its covalent feature in both of ferric and ferrous heme.

Conflicts of interest

There are no conflicts to declare.

Acknowledgements

The support of research council of University of Isfahan is appreciated. We also acknowledge extended discussions and valuable comments received from Professor Niloufar Shafizadeh and Professor Benoit Soep (University of Paris Saclay). We thank GENCI for a generous time allocation on the CINES supercomputers (project number hcp6830).

References

1 C. J. Reedy and B. R. Gibney, *Chem. Rev.*, 2004, **104**, 617–650.
2 H. B. Gray and J. R. J. Winkler, *Annu. Rev. Biochem.*, 1996, **65**, 537–561.
3 H. B. Dunford, *Peroxidases and catalases: biochemistry, biophysics, biotechnology and physiology*, John Wiley & Sons, 2010.
4 P. Harrison and E. J. Huehns, *Nature*, 1979, **279**, 476–477.
5 S. Yoshikawa, in *Handbook of Copper Pharmacology and Toxicology*, Springer, 2002, pp. 131–152.
6 B. A. Springer, S. G. Sligar, J. S. Olson and G. N. J. J. Phillips, *Chem. Rev.*, 1994, **94**, 699–714.
7 J. B. Wittenberg and B. A. J. Wittenberg, *J. Exp. Biol.*, 2003, **206**, 2011–2020.
8 S.-i. Ozaki, M. P. Roach, T. Matsui and Y. J. Watanabe, *Acc. Chem. Res.*, 2001, **34**, 818–825.
9 N. Lehnert, M. G. I. Galinato, F. Paulat, G. B. Richter-Addo, W. Sturhahn, N. Xu and J. Zhao, *Inorg. Chem.*, 2010, **49**, 4133–4148.
10 J. S. Olson and G. N. J. Phillips Jr, *J. Biol. Inorg Chem.*, 1997, **2**, 544–552.
11 E. A. Brucker, J. S. Olson, M. Ikeda-Saito and G. N. Phillips Jr, *Proteins: Struct., Funct., Bioinf.*, 1998, **30**, 352–356.
12 C. R. Andrew, S. J. George, D. M. Lawson and R. R. Eady, *Biochem*, 2002, **41**, 2353–2360.
13 L. M. Blomberg, M. R. Blomberg and P. E. J. Siegbahn, *J. Inorg. Biochem.*, 2005, **99**, 949–958.
14 L. E. Goodrich, F. Paulat, V. Praneeth and N. Lehnert, *Inorg. Chem.*, 2010, **49**, 6293–6316.
15 M.-S. Liao, M.-J. Huang and J. D. Watts, *J. Phys. Chem. B*, 2013, **117**, 10103–10114.
16 T. G. Spiro, A. V. Soldatova and G. Balakrishnan, *Coord. Chem. Rev.*, 2013, **257**, 511–527.

17 V. Praneeth, F. Paulat, T. C. Berto, S. D. George, C. Näther, C. D. Sulok and N. Lehnert, *J. Am. Chem. Soc.*, 2008, **130**, 15288–15303.
18 A. P. Hunt and N. Lehnert, *Acc. Chem. Res.*, 2015, **48**, 2117–2125.
19 M.-S. Liao, M.-J. Huang and J. D. J. Watts, *Mol. Phys.*, 2011, **109**, 2035–2048.
20 V. E. Berryman, R. J. Boyd and E. R. Johnson, *J. Chem. Theory Comput.*, 2015, **11**, 3022–3028.
21 V. E. Walker, N. Castillo, C. F. Matta and R. J. Boyd, *J. Phys. Chem. A*, 2010, **114**, 10315–10319.
22 M. Aarabi, R. Omidyan, S. Soorkia, G. Grégoire, M. Broquier, M.-E. Crestoni, A. de La Lande, B. Soep and N. Shafizadeh, *Phys. Chem. Chem. Phys.*, 2019, **21**, 1750–1760.
23 J. Vojtěchovský, K. Chu, J. Berendzen, R. M. Sweet and I. J. Schlichting, *Biophys. J.*, 1999, **77**, 2153–2174.
24 K. P. Kepp and P. J. Dasmeh, *J. Phys. Chem. B*, 2013, **117**, 3755–3770.
25 M. Aarabi, S. Soorkia, G. Grégoire, M. Broquier, A. de la Lande, B. Soep, R. Omidyan and N. J. Shafizadeh, *Phys. Chem. Chem. Phys.*, 2019, **21**, 21329–21340.
26 V. Praneeth, F. Neese and N. Lehnert, *Inorg. Chem.*, 2005, **44**, 2570–2572.
27 A. M. Koster, G. Geudtner, P. Calaminici, M. E. Casida, V. D. Dominguez, R. Flores-Moreno, G. U. Gamboa, A. Goursot, T. Heine, A. Ipatov, F. Janetzko, J. M. del Campo, J. U. Reveles, A. Vela, B. Zuniga-Gutierrez, and D. R. Salahub, *deMon2k, Version 6.1.7, the deMon developers, Cinvestav*, México, D.F.
28 M. Krack and A. M. J. Köster, *J. Chem. Phys.*, 1998, **108**, 3226–3234.
29 M. Swart, A. W. Ehlers and K. J. Lammertsma, *Mol. Phys.*, 2004, **102**, 2467–2474.
30 A. Goursot, T. Mineva, R. Kevorkyants and D. J. Talbi, *J. Chem. Theory Comput.*, 2007, **3**, 755–763.
31 E. R. Johnson and A. D. J. Becke, *J. Chem. Phys.*, 2017, **146**, 211105.
32 M. Frisch, M. Head-Gordon and J. Pople., *J. Chem. Phys.*, 1990, **141**, 189–196.
33 V. Barone and M. Cossi, *J. Phys. Chem. A*, 1998, **102**, 1995–2001.
34 S. F. Boys and F. J. Bernardi, *Mol. Phys.*, 1970, **19**, 553–566.
35 S. Grimme, S. Ehrlich and L. J. Goerigk, *J. Comput. Chem.*, 2011, **32**, 1456–1465.
36 K. Falahati, H. Tamura, I. Burghardt and M. J. Huix-Rotllant, *Nat. Commun.*, 2018, **9**, 1–8.
37 C. Rovira, K. Kunc, J. Hutter, P. Ballone and M. J. Parrinello, *J. Phys. Chem. A*, 1997, **101**, 8914–8925.
38 M. Radon and K. J. Pierloot, *J. Phys. Chem. A*, 2008, **112**, 11824–11832.
39 R. Bader and T. Nguyen-Dang, in *Adv. Quantum Chem.*, Elsevier, 1981, vol. 14, pp. 63–124.
40 T. A. Keith, *AIMAll (Version10.05.04)*, 2010, aim.tkgristmill.com.
41 W. R. Scheidt and M. E. Frisse, *J. Am. Chem. Soc.*, 1975, **97**, 17–21.
42 W. R. Scheidt and P. L. Piciulo, *J. Am. Chem. Soc.*, 1976, **98**, 1913–1919.
43 W. R. Scheidt, H. F. Duval, T. J. Neal and M. K. Ellison, *J. Am. Chem. Soc.*, 2000, **122**, 4651–4659.
44 G. R. Wyllie, C. E. Schulz and W. R. Scheidt, *Inorg. Chem.*, 2003, **42**, 5722–5734.
45 M. A. Martí, L. Capece, A. Crespo, F. Doctorovich and D. A. Estrin, *J. Am. Chem. Soc.*, 2005, **127**, 7721–7728.
46 M. A. Marti, L. Capece, A. Bidon-Chanal, A. Crespo, V. Guallar, F. J. Luque and D. A. Estrin, *Methods Enzymol.*, 2008, **437**, 477–498.
47 O. Chen, S. Groh, A. Liechty and D. P. Ridge, *J. Am. Chem. Soc.*, 1999, **121**, 11910–11911.
48 B. A. Springer, K. Egeberg, S. Sligar, R. Rohlfs, A. Mathews and J. J. Olson, *J. Biol. Chem.*, 1989, **264**, 3057–3060.
49 P. E. Siegbahn, M. R. Blomberg and S.-L. Chen, *J. Chem. Theory Comput.*, 2010, **6**, 2040–2044.
50 V. Praneeth, C. Näther, G. Peters and N. Lehnert, *Inorg. Chem.*, 2006, **45**, 2795–2811.
51 S. J. Grabowski, *Chem. Rev.*, 2011, **111**, 2597–2625.
52 W. R. Scheidt, Y. J. Lee and K. Hatano, *J. Am. Chem. Soc.*, 1984, **106**, 3191–3198.
53 A. B. McQuarters, J. W. Kampf, E. E. Alp, M. Hu, J. Zhao and N. Lehnert, *Inorg. Chem.*, 2017, **56**, 10513–10528.
54 F. Paulat and N. Lehnert, *Inorg. Chem.*, 2007, **46**, 1547–1549.
55 D. P. Linder, K. R. Rodgers, J. Banister, G. R. Wyllie, M. K. Ellison and W. R. Scheidt, *J. Am. Chem. Soc.*, 2004, **126**, 14136–14148.
56 A. V. Soldatova, M. Ibrahim, J. S. Olson, R. S. Czernuszewicz and T. G. Spiro, *J. Am. Chem. Soc.*, 2010, **132**, 4614–4625.
57 B. Chiavarino, M. E. Crestoni, S. Fornarini and C. Rovira, *Inorg. Chem.*, 2008, **47**, 7792–7801.